TISSUE SEGMENTATION OF MRSI DATA USING CANONICAL CORRELATION ANALYSIS

T. Laudadio KULeuven, Belgium
P. Pels KULeuven, Belgium
L. De Lathauwer ETIS, France
P. Van Hecke KULeuven, Belgium
S. Van Huffel KULeuven, Belgium

ABSTRACT

In this paper we present an accurate and efficient tissue segmentation technique based on Canonical Correlation Analysis, a statistical method able to simultaneously exploit the temporal and spatial information characterizing the Magnetic Resonance Spectroscopic Imaging (MRSI) data. Recently, Canonical Correlation Analysis has been successfully applied to other types of biomedical data, such as functional Magnetic Resonance Imaging data. Here, we adapt this method for MRSI data processing in order to retrieve in an accurate and efficient way the possible tissue types that characterize the organ under investigation. The potential and limitations of the new technique have been investigated by using simulated prostate MRSI data, and our studies demonstrate a high accuracy, robustness and efficiency.

Keywords: magnetic resonance spectroscopic imaging, canonical correlation analysis, tissue segmentation.

INTRODUCTION

Nowadays, MRSI represents a powerful non-invasive diagnostic tool. The ability of Magnetic Resonance Spectroscopy to detect metabolites is already very useful in daily radiological practice since it provides significant biochemical information on the molecules of the organism under investigation. MRSI data can also be exploited in tissue segmentation techniques, which play a crucial role in many biomedical applications such as the quantification of tissue volumes, localization of possible pathologies, improvement of pre-surgical diagnosis and optimization of the surgical approach, therapy planning, etc. A variety of methods are available in the literature. They are often used in combination in order to solve different segmentation problems. They can be divided into several categories: thresholding techniques, Sahoo et al. (1); region growing techniques, Mangin et al. (2); clustering techniques, Boleman and Andrews (3); Markov random field models, Held et al. (4); classifiers, Bezdek et al. (5); artificial neural networks, Reddick et al. (6); etc. In this paper, we propose a fast and reliable tissue segmentation technique which is based on a statistical method called Canonical Correlation Analysis (CCA). This method is the multivariate variant of the ordinary correlation analysis and has already been successfully applied to functional Magnetic Resonance Imaging data in order to map sensor, motor and cognitive functions to specific areas in the brain, Friman (7). Here we adapt CCA for MRSI data processing in order to detect possible homogeneous tissue regions characterizing the considered sample. The goal is achieved by combining the temporal-spatial information provided by the MRSI data set and the subspace modeling of characteristic tissue spectra. More precisely, CCA quantifies the relationship between two sets of variables, magnitude spectra of the measured data and signal subspace, by means of correlation coefficients. These coefficients are afterwards exploited in order to construct nosologic images in which all the detected tissues are visualized. Such images can be easily interpreted by radiologists and physicians and, along with clinical and radiological information, can improve the accuracy of the diagnosis. The paper is organized as follows: in the "Canonical Correlation Analysis" section a theoretical description of CCA is given. In the section entitled "CCA applied to MRSI data" the application of CCA to MRSI data is described. In the "Simulation studies" section extensive simulation studies are reported and the performance of the ordinary correlation analysis and its multivariate variant CCA are compared in terms of accuracy and efficiency. Finally, in the "Conclusions" section we formulate the main conclusions.

CANONICAL CORRELATION ANALYSIS

CCA is a statistical technique developed by Hotelling in 1936 in order to assess the relationship between two sets of variables, Hotelling (8). It is a multichannel generalization of ordinary correlation analysis, which quantifies the relationship between two random variables x and y by means of the so-called correlation coefficient ρ:

$$\rho = \frac{Cov[x, y]}{\sqrt{V[x]V[y]}}, \qquad [1]$$

which is a scalar with value between -1 and 1 that measures the degree of linear dependence between x and y. For zero-mean variables [1] is replaced by:

$$\rho = \frac{E[xy]}{\sqrt{E[x^2]E[y^2]}}. \qquad [2]$$

Canonical correlation analysis can be applied to multichannel signal processing as follows: consider two zero-mean multivariate random vectors $x=[x_1(t),\ldots,x_m(t)]^T$ and $y=[y_1(t),\ldots,y_n(t)]^T$, with $t=1,\ldots,N$, and the following linear combinations of the components in x and y, which respectively represent two new scalar random variables X and Y:

$$X = \omega_{x_1} x_1 + \cdots + \omega_{x_m} x_m = \omega_x^T x$$
$$Y = \omega_{y_1} y_1 + \cdots + \omega_{y_n} y_n = \omega_y^T y \qquad [3]$$

CCA computes the linear combination coefficients ω_x and ω_y, called regression weights, so that the correlation between the new variables X and Y is maximum. The solution $\omega_x=\omega_y=0$ is not allowed and the new variables X and Y are called canonical variates. It has been proved that computing the regression weights reduces to solving an eigenvalue problem, in which the eigenvectors represent the regression weights and the corresponding eigenvalues are called canonical coefficients. More precisely, as described in Golub and Zha (9), the regression weights and the corresponding canonical coefficients can be computed by solving the following symmetric generalized eigenvalue problem:

$$\begin{pmatrix} 0 & C_{xy} \\ C_{xy}^T & 0 \end{pmatrix} \begin{pmatrix} \omega_x \\ \omega_y \end{pmatrix} = \begin{pmatrix} C_{xx} & 0 \\ 0 & C_{yy} \end{pmatrix} \begin{pmatrix} \omega_x \\ \omega_y \end{pmatrix} \lambda, \quad [4]$$

subject to:

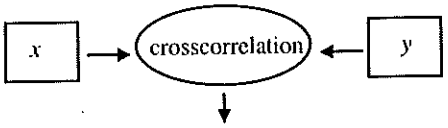
$$\begin{cases} \omega_x^T C_{xx} \omega_x = 1 \\ \omega_y^T C_{yy} \omega_y = 1 \end{cases} \qquad [5]$$

where C_{xx} and C_{yy} are the within-set covariance matrices of x and y, respectively, and C_{xy} is the between-sets covariance matrix. In practice, sample covariance matrices are used:

$$\hat{C}_{xx} = \frac{1}{N} \sum_{t=1}^{N} x(t) x(t)^T$$
$$\hat{C}_{yy} = \frac{1}{N} \sum_{t=1}^{N} y(t) y(t)^T \qquad [6]$$
$$\hat{C}_{xy} = \frac{1}{N} \sum_{t=1}^{N} x(t) y(t)^T$$

CCA APPLIED TO MRSI DATA

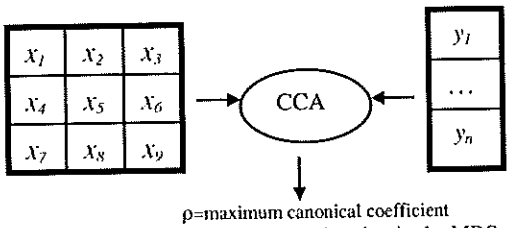
During the MRSI data acquisition procedure, a number of image slices is acquired. Each image can be partitioned into a certain number of volume elements, called voxels, each characterized by a time-domain signal of length N. In our tissue segmentation approach, the aim is to detect those voxels whose spectra correlate best with model tissue spectra, which are known a priori. When applying correlation analysis to MRSI data, we need to specify the variables x and y. In ordinary correlation analysis x and y are univariate variables and, specifically, the x variable consists of the magnitude spectrum of the measured signal contained in each voxel, while the y variable consists of the model tissue spectrum. The correlation coefficient between x and y is computed and, afterwards, assigned to the voxel under investigation. Once each voxel has been processed, a new grid of voxels, of the same size of the original image, is obtained, which contains correlation coefficients instead of MRSI signals. This new grid is called correlation map. Figure 1 schematically shows the ordinary correlation analysis approach.



ρ=correlation coefficient

Figure 1. Crosscorrelation between the measured magnitude spectrum x and the model spectrum y.

The difference between ordinary correlation analysis and CCA mainly consists in a different choice of the variables x and y. In fact, in order to compute the correlation maps, it is possible to exploit the spatial information characterizing the MRSI data set by considering, as variable x, a multivariate vector with components representing the spectrum characterizing the considered voxel as well as the spectra contained in the neighbor voxels. Several spatial models can be adopted in order to choose the neighbor voxels, the most significant examples of which are described in (7). Concerning the variable y, it also consists of a multivariate vector whose components represent the basis functions of a signal subspace, that models the characteristic tissue spectrum we are looking for and its possible variations (in amplitudes, frequency shifts and damping factors) that normally affect realistic MRSI data. Several approaches can be adopted in order to model a proper signal subspace; an exhaustive overview is given in (7). Once the x and y variables have been defined, CCA is applied voxel by voxel and the largest canonical coefficient is assigned to the voxel under investigation, so that a correlation map is obtained as in the ordinary correlation analysis case. Figure 2 schematically shows the CCA approach when processing a 3x3 voxel region containing the magnitude spectrum x_5 along with its neighbor spectra. In this particular spatial model, called the "3x3 model", the variable x contains nine components, namely $x=[x_1(t),\ldots,x_9(t)]^T$.



ρ=maximum canonical coefficient

Figure 2. CCA between a 3x3 voxel region in the MRS image and a set of n basis functions.

SIMULATION STUDIES

Figure 3 shows the magnitude spectra of four different simulated signals, derived from in vivo data measured in the human prostate, representing very aggressive tumor tissue, moderately aggressive tumor tissue, mixed tumor tissue, and healthy peripheral zone tissue.
As it is possible to observe in the above mentioned figure, the spectra are characterized by the presence of three metabolite peaks: Choline, Creatine and Citrate doublet. In particular, aggressive tumor tissue is characterized by a strong contribution of Choline, while healthy tissue exhibits a higher contribution of Citrate. In general, prostate tumor regions are characterized by higher levels of Choline and reduced levels of Citrate.

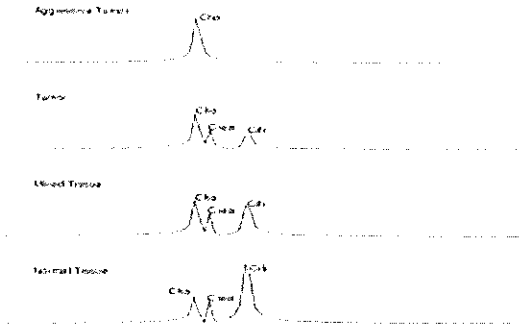


Figure 3. Magnitude spectra of characteristic prostate signals

The spectra represent the Discrete Fourier Transform of four signals modeled as the sum of $K=4$ exponentially damped complex sinusoids:

$$s_n = \sum_{k=1}^{K} a_k e^{j\phi_k} e^{(-d_k + j2\pi f_k)t_n}, \quad n = 1,\ldots,N \qquad [6]$$

where s_n represents the n^{th} datapoint of the simulated signal; j represents the imaginary unit; the parameters a_k, ϕ_k, d_k and f_k denote the amplitude, phase, damping factor and frequency, respectively; $t_n=t_0+n\Delta t$, with Δt the sampling interval and t_0 the time between the effective time origin and the first data point to be included in the analysis. The parameter values of the noiseless simulated signals are reported in Table 1, where the abbreviations AT, T, M, H respectively denote aggressive tumor, tumor, mixed, and healthy tissue. The dampings and frequencies were selected based on in vivo prostate data acquired at 1.5T. The Citrate was modeled as a doublet with frequency split equal to 2.5Hz. The amplitude values are expressed in arbitrary units.

A simulated MRSI data set was produced, consisting of a 14x14 grid of voxels, in which four different and well localized regions of tissue spectra were inserted. The grid is shown in Figure 4 and the tissue regions are indicated by different colors: brown for aggressive tumor tissue, red for tumor tissue, orange for mixed tissue and light blue for healthy tissue

TABLE 1-Parameter values of the simulated signals

Parameters		Choline	Creatine	Citr1	Citr2
f_k (Hz)		-49.3	-38.9	-12.1	-9.6
d_k (Hz)		2	2	2	2
Φ_k (°)		0	0	0	0
a_k	AT	4.3e6	0.2e6	0.2e6	0.2e6
	T	3.3e6	1.6e6	1.2e6	1.2e6
	M	3.3e6	1.8e6	2.4e6	2.4e6
	H	2.3e6	1.8e6	4.4e6	4.4e6

Figure 4. Original tissue grid

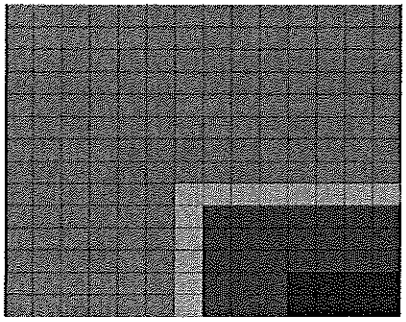


Figure 5 shows the spectra contained in the previous grid. In order to simulate a realistic MRSI data set, variations were introduced on the signal parameters displayed in Table 1. More precisely, spectra for each type of tissue were generated, randomly characterized by variations up to 20% for amplitudes, up to twenty times the given value for the damping factors, up to 1.25Hz for the frequencies.

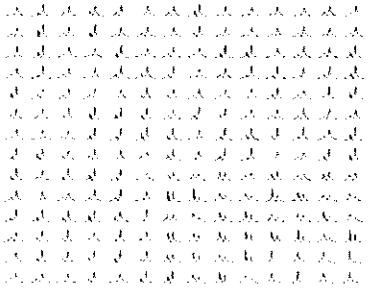


Figure 5. Simulated MRSI spectra

The magnitude spectra of the simulated signals were perturbed by adding Gaussian noise with standard deviation σ. Ordinary correlation analysis and CCA were then applied in order to detect the four tissue regions.

Choice of the spatial model

As already mentioned in the previous section, several spatial models can be chosen when applying CCA. As a particular case, the ordinary correlation analysis can be considered as a single-voxel model. We investigated the performance of the following spatial models:
- the single-voxel model (see Figure 1)
- the 3x3 model (see Figure 2)
- the 3x3 model without corner voxels ($x=[x_2(t), x_4(t), x_5(t), x_6(t), x_8(t)]^T$)
- the symmetric 3x3 model ($x=[x_5(t), (x_1(t)+ x_9(t))/2, (x_2(t)+ x_8(t))/2, (x_3(t)+ x_7(t))/2, (x_4(t)+ x_6(t))/2\ ]^T$)
- the symmetric 3x3 model without corner voxels ($x=[x_5(t), (x_2(t)+ x_8(t))/2, (x_4(t)+ x_6(t))/2\ ]^T$)

The obtained results are described in the "simulation results" section.

Choice of the subspace model

Concerning the choice of the y variable, we considered two different approaches in order to define the proper signal subspace able to model the characteristic tissue spectra and their possible variations. Specifically, we considered the Taylor model and the Principal Component Analysis model.
The Taylor subspace model consists of choosing as first component of the variable y, the magnitude spectrum of the noiseless simulated signal without any variation on the parameters. As second and third components, we consider the first-order derivative of the first component, approximated by first-order and second-order finite differences, respectively. More precisely, let us consider one of the magnitude spectra reported in Figure 3 and denote it by $S(\omega_n)$, where ω_n represents the frequency and $n=1,\ldots,N$. Then, the components of the y variable are given by:

$$\begin{cases} y_1(n) = S(\omega_n) \\ y_2(n) = \dfrac{S(\omega_{n+1}) - S(\omega_n)}{\Delta\omega} \\ y_3(n) = \dfrac{S(\omega_{n+1}) - S(\omega_{n-1})}{2\Delta\omega} \end{cases} \quad [7]$$

where $\Delta\omega$ is the sampling frequency.
The Principal Component Analysis subspace model is obtained by producing a high number of signals characterized by realistic variations on the noiseless simulated signal parameters. The first component of the y variable is given by the mean of the magnitude spectra of the produced signals, while the second component is given by the first Principal Component which is obtained by performing Principal Component Analysis on the matrix containing the magnitude spectra of the mean-centered signals. The aforementioned procedure, for one tissue type, can be schematically described as follows:

1. Compute the simulated noiseless signal corresponding to the considered tissue type (with parameters reported in Table 1) and its magnitude spectrum $S(\omega_n)$.
2. Produce a high number M of signals by introducing realistic variations on the noiseless signal parameters of the chosen tissue type.
3. Compute the magnitude spectra $S_i(\omega_n)$, $i=1,\ldots,M$, of the M signals produced in the previous step and arrange them as rows into a matrix D.
4. Perform Principal Component Analysis on the matrix D and denote the first Principal Component as $1^{st}PC$.
5. Set the components of the variable y as:

$$\begin{cases} y_1(n) = \dfrac{1}{M}\sum_{i=1}^{M} S_i(\omega_n) \\ y_2(n) = 1^{st}\,PC \end{cases} \quad [8]$$

Simulation results

In our simulation studies 300 simulation runs were performed for different noise standard deviation values. Before applying the proposed tissue segmentation method, four different y variables were defined, one for each prostate tissue type. CCA was then applied between the noisy data set and the above mentioned y variables, and four correlation maps were obtained. The nosologic image, consisting of one single image in which all the detected tissue types are visualized, was obtained by comparing, voxel by voxel, the four canonical coefficients characterizing the different correlation maps. The considered voxel was then assigned to the tissue with highest canonical coefficient and labeled by the corresponding tissue color.
In order to compare the performance of CCA when applying different spatial models and/or different subspace models, the correlation coefficients between the original and the detected tissue regions were estimated for each simulation run.
Figure 6 and Figure 7 shows the mean values of these correlation coefficients, over the total number of simulation runs and for each noise level, for different spatial models and by considering the PCA subspace model. The red line represents the single voxel model (sv); the green line represents the 3x3 model (3x3); the black line represents the 3x3 model without corner voxels (3x3wcv); the magenta line denotes the symmetric 3x3 model (sym3x3) and the blue line represents the symmetric 3x3 model without corner voxels (sym3x3wcv). As it is possible to observe in the figure, the best performance is provided by the symmetric 3x3 model, while the single voxel model

performs worst, especially for high noise levels. In general, the performance of all models is sensitive to the number of voxels characterizing the original tissue region as well as the shape of the spectra. In fact, the quality of the performance for the mixed tissue region is much poorer with respect to the performance shown for the other tissue regions, since little spatial information is exploited and the level of the different metabolites in the spectra is not as discriminating as in the other tissue spectra.

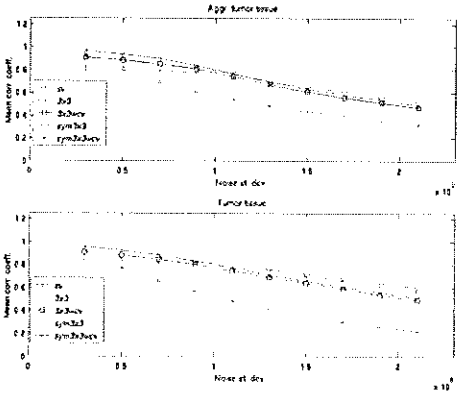


Figure 6. Mean of the correlation coefficients, over 300 simulation runs, between the detected tissue regions and the original tissue regions, vs the noise standard deviation, when considering different spatial models. Tissue types: aggressive tumor (top), tumor (bottom)

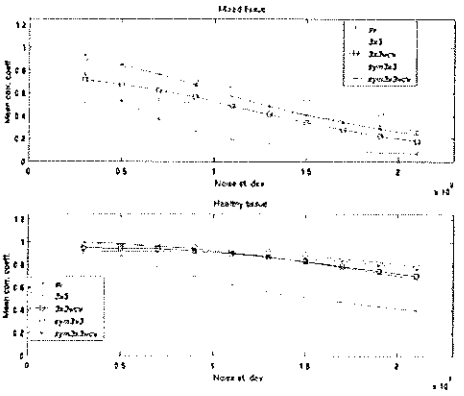


Figure 7. Mean of the correlation coefficients, over 300 simulation runs, between the detected tissue regions and the original tissue regions vs the noise standard deviation, when considering different spatial models. Tissue types: mixed (top), healthy (bottom)

In Figure 8 the mean values of the computation times, as a function of the noise standard deviation and over the total number of simulation runs, are displayed. The single voxel model is the most efficient, but the other models can be considered efficient as well since they only require less than 1 second (except for the 3x3 model) in order to process the whole simulated MRSI data set.

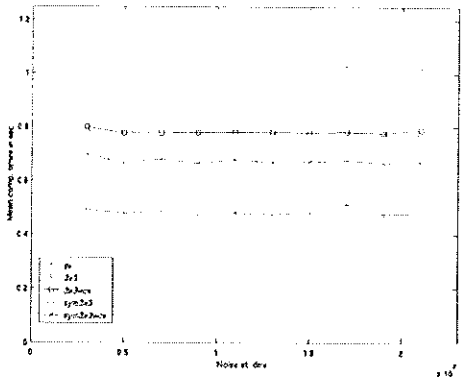


Figure 8. Mean of the computation times (in seconds), over 300 simulation runs and as a function of the noise standard deviation

Figure 9 shows the comparison between the PCA and the Taylor subspace models when applying the symmetric 3x3 spatial model. The magenta line represents the PCA model (PCA), while the blue line represents the Taylor model (Taylor). The PCA subspace model clearly outperforms the Taylor approach for the aggressive tumor, tumor and mixed tissue regions, while the behavior is similar for the healthy tissue region.

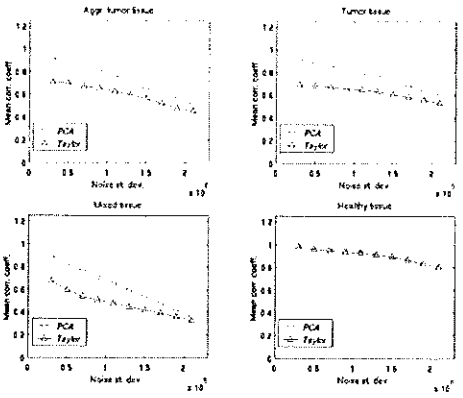


Figure 9. Comparison between the PCA and Taylor models in terms of correlation coefficient means

Concerning the comparison between the computation times, the Taylor model is slightly less efficient than the PCA approach, as shown in Figure 10, since it makes use of one more component in the y variable.

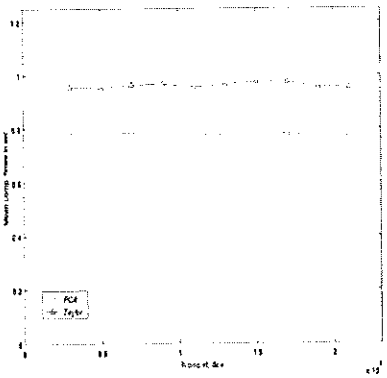


Figure 10. Comparison between the PCA and Taylor models in terms of computation times

As final result of our study, we show the regions detected by the single voxel model and the symmetric 3x3 model when considering a high noise level (noise standard deviation = $110*10^6$). The subspace model is based on the PCA approach. Figure 11 shows the nosologic image obtained by applying the single voxel approach, while Figure 12 provides the detection results obtained by the symmetric 3x3 model approach. The images clearly show that the multi-voxel approach significantly outperforms the ordinary correlation analysis approach. In fact, the tissue regions detected by CCA are well localized, despite their irregular edges. On the other hand, the single voxel approach detects the presence of aggressive tumor and mixed tissue voxels in parts of the grid where only healthy tissue spectra were originally inserted.

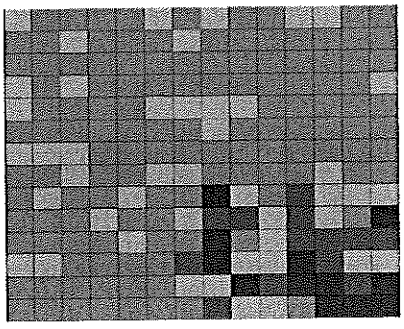


Figure 11. Nosologic image obtained by the single voxel model

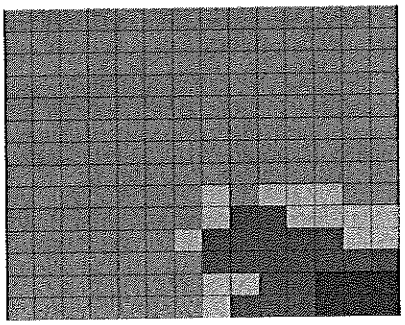


Figure 12. Nosologic image obtained by the symmetric 3x3 multi-voxel model

CONCLUSIONS

CCA is a statistical technique that quantifies the relationship between multivariate random vectors. Our studies show that it can be successfully applied to MRSI data sets since it fully exploits the spatio-temporal nature of this type of biomedical data. In particular, CCA can be applied to MRSI data in order to retrieve in an efficient and accurate way the possible tissue types characterizing the organ under investigation. Extensive simulation studies show that CCA significantly outperforms the ordinary correlation analysis, especially for signals with a low Signal to Noise Ratio.

ACKNOWLEDGMENTS

Dr. Sabine Van Huffel is a full professor at the Katholieke Universiteit Leuven, Belgium. Research supported by Research Council KUL: GOA-MEFISTO 666 and GOA-AMBioRICS, several PhD/postdoc & fellow grants; Flemish Government: FWO: PhD/postdoc grants, projects, G.0407.02 (support vector machines), G.0269.02 (magnetic resonance spectroscopic imaging), G.0270.02 (nonlinear Lp approximation), G.0360.05 (EEG signal analysis for epilepsy monitoring), research communities (ICCoS, ANMMM); IWT: PhD Grants, Belgian Federal Government: DWTC (IUAP IV-02 (1996-2001) and IUAP V-22 (2002-2006): Dynamical Systems and Control: Computation, Identification & Modelling)); EU: PDT-COIL (contract no. NNE5/2001/887), BIOPATTERN (contract no. FP6-2002-IST 508803) , ETUMOUR (contract no. FP6-2002-LIFESCIHEALTH 503094).

REFERENCES

1. Sahoo P.K., Soltani S., and Wong A.K.C., 1988, Comput. Vis. Graph. Im. Proc., 41, 233-260

2. Mangin J.F., Frouin V., Bloch I., Regis J., and Lopez-

Krahe, 1995, J. Math. Imag. Vis., 5, 297-318

3. Boleman G.B., and Andrews H.C., 1979, Proc. IEEE, 5, 773-785

4. Held K., Kops E.R., Krause B.J., Wells W.M., Kikinis R. et al., 1997, IEEE T. Med. Imag., 16 (6)

5. Bezdek J.C., Hall L.O., and Clarke L.P., 1993, Med. Phys., 20, 1033-1048

6. Reddick W.E., Glass J.O., Cook E.N., Elkin T.D., and Deaton R.J., 1997, IEEE T. Med. Imag., 16, 911-918

7. Friman O., 2003, PhD thesis, Dept. Biomed. Engin. Linköpings Univ., Sweden

8. Hotelling H., 1936, Biometrika, 28, 321-377

9. Golub G.H., and Zha H., 1995, "Linear Algebra for signal processing", A. Bojanczyk and G. Cybenco eds., Springer, New York, 59-82